INLAND WATERS
2019, VOL. 9, NO. 2, 162–176
https://doi.org/10.1080/20442041.2019.1568073

Implications of river intrusion and convective mixing on the spatial and temporal variability of under-ice CO_2

Natacha Pasche [a,b], Hilmar Hofmann [c], Damien Bouffard [b,d], Carsten J. Schubert [d], Petr A. Lozovik [e], and Sebastian Sobek [f]

[a]Limnology Center, EPFL-ENT-LIMNC, Lausanne, Switzerland; [b]Physics of Aquatic Systems Laboratory, Margaretha Kamprad Chair, EPFL-ENAC-IEE-APHYS, Lausanne, Switzerland; [c]Environmental Physics Group, University of Konstanz - Limnological Institute, Konstanz, Germany; [d]Eawag, Swiss Federal Institute of Aquatic Science and Technology, Department of Surface Waters-Research and Management, Kastanienbaum, Switzerland; [e]Northern Water Problems Institute, Karelian Research Center, Russian Academy of Sciences, Petrozavodsk, Russia; [f]Department of Ecology and Genetics, Limnology, Uppsala University, Uppsala, Sweden

ABSTRACT

Ice-covered periods might significantly contribute to lake emissions at ice-melt, yet a comprehensive understanding of under-ice carbon dioxide (CO_2) dynamics is still lacking. This study investigated the processes driving spatiotemporal patterns of under-ice CO_2 in large Lake Onego. In March 2015 and 2016, under-ice CO_2, dissolved inorganic carbon (DIC), and dissolved organic carbon (DOC) distributions were measured along a river to an open-lake transect. CO_2 decreased from 120/129 µmol L^{-1} in the river to 51/98 µmol L^{-1} in the bay, and 34/36 µmol L^{-1} in the open lake, while DOC decreased from 1.18/1.55 mmol L^{-1} in the river to 0.67/1.04 mmol L^{-1} in the bay in 2015 and 2016, respectively. These decreases in concentrations with increasing distance from the river mouth indicate that river discharge modulates spatial patterns of under-ice CO_2. The variability between the 2 years was mainly driven by river discharge and ice transparency affecting the extent of under-ice convection. Higher discharge during winter 2016 resulted in higher CO_2 concentrations in the bay. By contrast, intensive under-ice convection led to lower, more homogeneously distributed CO_2 in 2015. In conclusion, the river-to-bay transition zone is characterized by strong CO_2 variability and is therefore an important zone to consider when assessing the CO_2 budget of large lakes.

ARTICLE HISTORY
Received 29 January 2018
Accepted 7 January 2019

KEYWORDS
carbon dioxide; convective mixing; humic lake; humic lake; river intrusion; spatial distribution; under-ice

Introduction

Inland waters are an important component of the global carbon cycle. Freshwater systems transport carbon toward the ocean, bury carbon in the sediment, and emit greenhouse gases (GHG), carbon dioxide (CO_2), and methane (CH_4) to the atmosphere (e.g., Tranvik et al. 2009). Although half of lakes worldwide are seasonally ice-covered, the ice-covered period has received little attention compared to the ice-free season (Hampton et al. 2015). Even if the ice-melt periods could contribute up to ~50% of the annual GHG emissions of seasonally ice-covered lakes (Karlsson et al. 2013, Denfeld et al. 2018), a comprehensive understanding of under-ice GHG dynamics is still lacking (Powers and Hampton 2016).

During winter, ice-covered lakes experience reduced hydrological inputs, low water temperatures, impeded air–water gas exchange, and highly heterogeneous light availability, which all affect under-ice GHG cycling. Because ice cover hinders the air–water gas exchange, CO_2 accumulation under ice is a ubiquitous feature of periodically frozen lakes. In addition, the ice quality and snow cover may limit solar radiation for photosynthetic CO_2 fixation (Leppäranta 2015) and generate under-ice convective mixing (Bouffard et al. 2016, Bouffard and Wüest 2019). In some cases, this convective mixing can efficiently homogenize CO_2 concentrations in the water column prior to the spring overturn (Baehr and De Grandpre 2004), reducing CO_2 emissions at ice-melt. Recent winter studies (Denfeld et al. 2015, Ducharme-Riel et al. 2015) indicate that the release of accumulated winter CO_2 is more dynamic than previously believed and might depend on vertical mixing, catchment inputs, and lake internal processes. However, the spatial and temporal sampling resolution of existing studies limits our understanding of under-ice CO_2 dynamics in lakes.

The scarcity of direct under-ice measurements results in a limited knowledge of the mechanisms driving spatial

CONTACT Natacha Pasche natacha.tofield-pasche@epfl.ch

and temporal patterns of CO_2 in winter. Baehr and DeGrandpre (2002, 2004) observed a high temporal variability in under-ice CO_2 measured at high frequency attributed to multiple sources, indicating that a better understanding of the balance among external inputs, internal consumption, and production processes is needed. Photosynthetic CO_2 fixation is commonly low in winter, although it can be substantial in some large clear lakes (Bizic'-Ionescu et al. 2014). Respiratory CO_2 production is often larger than photosynthesis, and net heterotrophic metabolism is typically an important source of CO_2 emitted from lakes to the atmosphere (Duarte and Prairie 2005). This heterotrophy is partly caused by mineralization of the terrestrially derived (allochthonous) organic carbon that fuels in-lake respiration (Sobek et al. 2003). Hydrological inputs of CO_2 and allochthonous carbon through river inflows, surface runoff, and groundwater might be especially large in late winter and early spring (Cortés et al. 2017). The spatial dynamics of CO_2 might therefore be pronounced in transitional zones from river to lakes.

On a landscape scale, rivers and streams may emit more CO_2 than lakes (Crawford et al. 2014). Kokic et al. (2015) showed that headwater streams can contribute up to 65% of the total aquatic CO_2 evasion of a lake catchment, even though streams covered <0.1% of the catchment area. The higher CO_2 supersaturation in rivers than lakes is mainly caused by their higher lateral exchange with the terrestrial environment (Duarte and Prairie 2005). Thus, CO_2 input by rivers accounts for an important fraction of the CO_2 budget in lakes (Maberly et al. 2012, Chmiel et al. 2016), suggesting that transition zones between rivers and lakes may be important hotspots for lake CO_2 emission. Although the importance of fluvial inputs to lakes have been frequently reported (Stets et al. 2009, Natchimuthu et al. 2017), transitional areas between rivers and lakes remain rarely investigated. This gap is even more pronounced during the ice-covered period.

To address this important gap, our study investigated under-ice CO_2 dynamics in large boreal Lake Onego using spatially and temporally extensive sampling along a river to open-lake transect during 2 consecutive years. Lake Onego is oligotrophic and rich in dissolved humic matter, a type of lake not considered in the Denfeld et al. (2018) review. Because boreal lakes were mostly investigated in North America and Fenno-Scandinavia, our study provides new insight into a lake currently located in an underrepresented region. While most winter investigations were limited to relatively small lakes, we studied the second largest lake in Europe within the multidisciplinary project "Life under ice." Our colleagues (Bouffard et al. 2019) assessed the convective mixing during our study period, and their results were used to interpret the patterns found in our study. The goal of our research was to quantify the temporal and spatial variability of under-ice CO_2 in the transition zone along a river to an open-lake transect. We hypothesized that (1) CO_2 concentrations decrease with increasing distance from the river mouth, and (2) temporal dynamics across days and years are driven by vertical mixing and horizontal transport within the water column.

Materials and methods

Site description

Lake Onego is situated in northwestern Russia at a latitude of 61–63°N and is usually covered by ice from mid-November to mid-May. This large lake has a surface area of 9720 km^2, a volume of 295 km^3 (Sabylina et al. 2010). Its mean and maximum depths are 30 and 120 m, respectively. The lake mixes twice a year, in autumn and spring. Lake Onego is oligotrophic, with total phosphorus (TP) <10 $\mu g\ L^{-1}$ in the open lake, and is characterized by soft and humic waters due to the high percentage of boreal forests and wetlands in the catchment. The major inflows are the Vodla, Shuya, and Suna rivers that account for 60% of the total riverine inputs to the lake (17.6 $km^3\ yr^{-1}$). The remaining riverine inputs are allocated to 52 rivers longer than 10 km and >1000 other smaller tributaries. Precipitation accounts for 5.4 $km^3\ yr^{-1}$.

In the western part of the lake, Petrozavodsk Bay (PB) is one of Lake Onego's largest bays, with a water surface area of 73 km^2 representing almost 1% of the total lake surface (Sabylina et al. 2010). The average and maximum depths of PB are 16 and 27 m, respectively. Petrozavodsk City, the capital of the Karelian Republic with ~270 000 inhabitants, is situated along the southwestern shore of PB. The main natural water input into PB is the River Shuya (RS), contributing 93% of the water input to PB (Podsechin et al. 2009). Water quality was analyzed in PB in the inflows and the open lake, and seasonal retention time was calculated using conservative tracers (Lozovik et al. 2007). These calculations showed that retention time in PB decreased from winter (2.9 months) to autumn (0.8 months), with an annual average of 1.6 months (Lozovik PA, Northern Water Problems Institute, unpubl. data). In winter, the water quality and properties in PB are therefore mainly influenced by the humic water of RS.

RS is the second largest tributary of Lake Onego, with a total length of 279 km and a catchment area of 10 000

km^2 (Podsechin et al. 2009). The river catchment is composed of 70% boreal forests, 19% wetlands, and 10% small lakes. Its annual runoff is about 3.09 km^3 yr^{-1}, representing 17.5% of all river inflow to Lake Onego (17.6 km^3 yr^{-1}). RS discharge is characterized by peak flows in May/June, reaching 56–426 m^3 s^{-1}, while winter flows from January to March are lowest, at ~8–103 m^3 s^{-1}.

Sampling sites

This study is part of the multidisciplinary project "Life under ice," which brought together 40 European and Russian scientists from across limnological fields including physics, chemistry, biology, sedimentology, and remote sensing. Two common field campaigns were conducted during the ice-covered period from 15 to 26 March 2015 and from 11 to 23 March 2016. An ice camp (IC) was installed in the center of PB, allowing discrete and continuous measurements day and night for most of the research groups (Fig. 1). Our sampling strategy was to study temporal patterns in under-ice CO_2 at the IC and to distinguish spatial patterns along a river to open-lake transect. To assess the under-ice conditions, the first measurements took place at IC collaboratively and were discussed among the different research groups. Based on these initial measurements, we selected the sampling depths and then used the same depths for subsequent sites. In 2015, sampling was conducted in RS, at IC in the bay center, and in a pelagic location (C3) under cracking and rapidly deteriorating ice conditions. Given the importance of the river to the bay, we decided in 2016 to increase the spatial resolution within the bay. Because ice conditions were safe, we sampled at the same sites sampled in 2015 and added 2 sites between the IC and the river mouth (PB1 and PB2) and 2 other sites between the IC and the bay edge (PB2.5 and PB3).

We summarized the sampling sites, ice and meteorological conditions, and the river discharge during both sampling campaigns (Table 1). Air temperature and precipitation were obtained from the meteorological station in Petrozavodsk City (https://rp5.ru/Weather_archive_in_Petrozavodsk) and water discharge from the hydrological station. The ice-covered period was assessed using images from the NASA satellites Terra (Filatov et al. 2019), whereas ice thickness and structure were

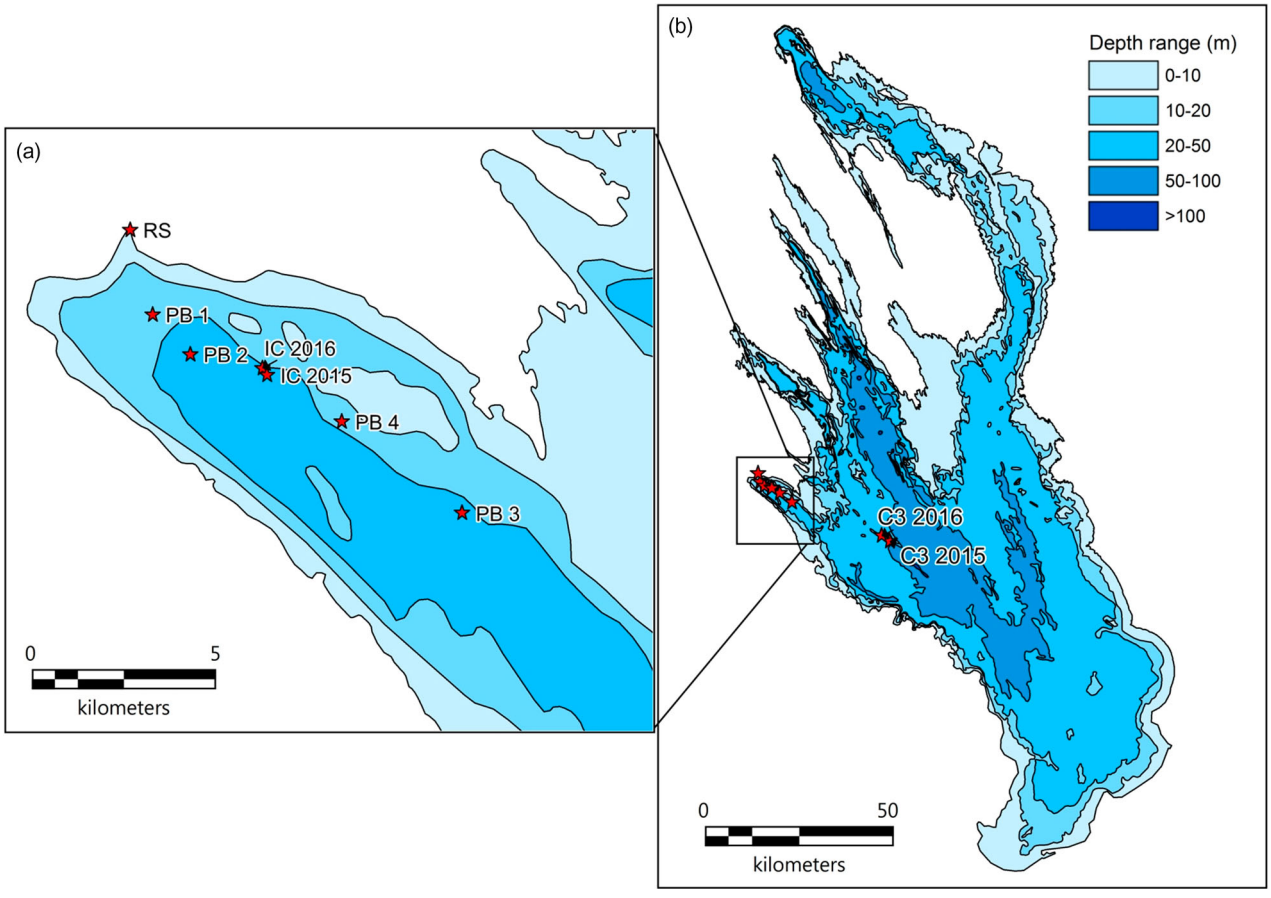

Figure 1. Bathymetry of Lake Onego, including sampling stations (red stars). (a) Petrozavodsk Bay area with sampling stations (red stars); (b) whole lake.

Table 1. Sampling sites in Lake Onego, river discharge, and meteorological and ice conditions during the 2 sampling campaigns. The euphotic depth and the depth of convective mixing were determined by Bouffard et al. (2019). RS = River Shuya; PB = Petrozavodsk Bay; IC = ice camp.

Description	March 2015	March 2016
Sampling sites	RS, IC 2015, C3 2015	RS, PB1, PB2, IC 2016, PB 2.5, PB 3, C3 2016
Sampling campaign	15–26 Mar	11–23 Mar
Ice thickness	26 to 40 cm	47 cm
Ice structure	transparent	First 10 cm of white ice, transparent below
Ice-covered period	13 Feb to 11 Apr	22 Jan to 23 Apr
River Shuya averaged discharge in March (m^3 s^{-1})	25.2	47.7
Average air temperature during campaign (°C)	−0.5	−2.7
Average precipitation during campaign (mm)	27.1	2.6
Euphotic depth (m)	4	1.5
Depth of convective mixing (m)	24	10

Table 2. Coordinates of sampling locations in Lake Onego with maximum depth and sampling dates. RS = River Shuya; PB = Petrozavodsk Bay; IC = ice camp.

Station Name	Sampling date	Location	Latitude N	Longitude E	Max depth (m)
RS	24 Mar 2015; 15 Mar 2016; 21 Mar 2016	river	61.84649	34.35762	5
PB1	15 Mar 2016; 21 Mar 2016; 22 Mar 2016	bay	61.82688	34.36992	20
PB2	17 Mar 2016; 21 Mar 2016	bay	61.81715	34.38940	22.5
IC 2015	22 Mar 2015; 25 Mar 2015	bay	61.81211	34.42908	27.5
IC 2016	16 Mar 2016; 18 Mar 2016; 20 Mar 2016	bay	61.81377	34.42667	27.5
PB2.5	21 Mar 2016; 23 Mar 2016	bay	61.80072	34.46778	23
PB3	14 Mar 2016; 21 Mar 2016; 23 Mar 2016	bay edge	61.77845	34.52995	29
C3 2015	17 Mar 2015	open lake	61.68539	35.02581	61
C3 2016	22 Mar 2016	open lake	61.69902	34.98402	42

determined directly in the field after removing an ice core. Bouffard et al. (2019) determined the depth of light extinction and the depth of convective mixing by in situ measurements.

Methods

At each sampling location, vertical profiles were taken in 2016 with a Sea and Sun probe (CTD75M; Trappenkamp, Germany) to record temperature, oxygen, conductivity, and turbidity. In 2015, the physicochemical profiles were taken with an YSI EXO 2 probe (Yellow Springs, OH, USA) recording oxygen and temperature. These profiles were used to select key depths for water sampling, dividing the other depths throughout the water column with an emphasis near the surface and the bottom.

Carbon measurements from water samples

Water samples were collected with a customized Ruttner water sampler. On 22 and 25 March 2015, 11 depths were selected at IC in 2015 (1, 3, 4, 10, 18, 22, 23, 24, 25, 26, and 27 m). In 2016, each site (Table 2) was usually sampled once for water samples and once for the CO_2 sensor but were sampled simultaneously for both methods on 18 March at IC and 23 March at C3. At least 8 depth levels per site were probed (0, 0.5, 1.5, 5, 9, 14, 20 m, and near bottom). On 21 March, an intense campaign took place on RS, PB1, PB2, PB2.5, and PB3 for dissolved organic carbon (DOC) and physicochemical profiles.

CO_2 and DIC

Because Lake Onego has an extremely low alkalinity and a pH ~6.3, the classic method from carbonate equilibria would have induced large uncertainties (Golub et al. 2017), so we used direct measurements of the partial pressure of CO_2 (pCO_2). For CO_2 and dissolved inorganic carbon (DIC), 60 mL syringes were immediately filled bubble-free in triplicate in the field, kept in a dark and cold cool-box, and analysed within 4 h the same day. For CO_2, the water volume in the syringes was adjusted to 30 mL, and a 30 mL headspace of ambient air was added. When adding this headspace, ambient air was collected in separate syringes to measure pCO_2 of ambient air. The gas and water phase were then equilibrated by shaking the syringes for 2 min (Denfeld et al. 2015). We measured pCO_2 with a portable infrared gas analyzer (EGM-4 Environmental Gas Analyzer, PP-Systems Inc., Amesbury, MA, USA), which has an accuracy of <1% of the calibrated range (0–5000 µatm). The measurement of DIC followed the same procedure, except that a 20 mL water volume in the syringe was acidified with 100 µL 3.7% HCl and a headspace of 40 mL was added. CO_2 and DIC concentrations in the water were calculated via Henry's constant (Weiss 1974) after correction for the atmospheric pressure and temperature during measurements, deducting the amount of CO_2 added to the headspace volume from the ambient air (Sobek et al. 2003, Karlsson et al. 2013, Denfeld et al. 2015). The uncertainty of the triplicate samples was <4.8%, calculated as the percentage of the standard deviation on the average value.

DOC

Water samples for dissolved organic carbon (DOC) were filtered at 0.45 µm, acidified with 3.7% HCl, and kept at 4 °C until analysis in the lab using a Shimadzu TOC-L (Columbia, MD, USA). DOC measurements had an accuracy of 0.2 mg L^{-1}.

High-frequency CO_2 measurements

In addition to the CO_2 measurements obtained from water samples, in situ CO_2 concentrations were measured with a CO_2 probe based on infrared absorption spectroscopy (HydroC CO_2, Contros Systems & Solutions GmbH, Germany) every 5 s. The Contros CO_2 sensor is calibrated by the manufacturer for several temperatures and concentrations between 0 and 25 °C and between 200 and 5000 µatm, respectively, and thus covered field conditions and data range. The conversion from µatm to µmol L^{-1} was calculated for in situ temperatures using Henry's law.

Discrete vertical profiles were measured at station IC on 22 and 25 March 2015, and on 18 and 20 March 2016, as well as at station PB1 and C3 on 22 March and at station PB3 and PB2.5 on 23 March in 2016. For the discrete vertical profiles, the CO_2 probe was lowered to the desired depth and maintained for 10–20 min at the same depth (response time $t_{63\%}$ is ~60 s). At each depth station, the last 30% of the time series (3–6 min) was averaged, representing the dissolved CO_2 concentration at that depth. CO_2 concentrations measured in situ with the CO_2 probe agreed within ±10% of the data obtained from water samples with the EGM-4 portable gas analyzer. An oxygen optode (MiniDOT, PME, Vista, CA, USA) and a combined temperature and depth logger (TDR, RBR, Ottawa, Canada) were always attached to the frame of the CO_2 probe to measure temperature, dissolved oxygen concentration, and water depth in combination with CO_2.

For continuous measurements, the CO_2 probe was deployed at 4.5 m depth from 17 to 18 March 2016, and at 11 m depth from 18 to 21 March 2016. The depth of 4.5 m was chosen in the convective layer and the depth of 11 m was selected after the initial profiling where maximum CO_2 concentrations were observed.

Interpolated maps

For a better data representation, interpolation maps were created using the specialized software Ocean Data View. For these maps, we selected the vertical profiles between 20 and 22 March for a better temporal integrity. For each map, the interpolation used the weighted average gridding method, with scale-lengths of 85 permil for X and 150 permil for Y. The same section along the river to open-lake transect was used for every map. Given the large distance (25.6 km) between PB3 and C3, the interpolated parameters have more uncertainties between these 2 stations than within PB. Similarly, the depth range was limited to 30 m to emphasize the bay area and to minimize interpolation errors.

Field observations

Convective mixed layer

Bouffard et al. (2019) investigated in detail under-ice convective mixing at IC, and we describe here only their key findings. The main driver for convective mixing is the solar radiation penetrating the water (Bouffard and Wüest 2019). Underwater photosynthetically active radiation (PAR) measurements showed light penetrating the water down to ~4 m in 2015 but only to ~1.5 m in 2016 (Table 1). This difference was first explained by the snow cover on the ice, drastically reducing light penetration into the water in 2016, even if the solar radiation was similar for both years. Second, the measured light absorption was larger in 2016 than in 2015, corresponding to a PAR attenuation coefficient (k_{PAR}) of 1.2 m^{-1} in 2015 and 3.2 m^{-1} in 2016. As a result, the extension of the convective layer differed significantly in both years. In 2015, the convective layer extended to a depth of ~24 m, whereas in 2016 the convective layer only extended to ~10 m depth. In addition, calculations (Bouffard et al. 2016, 2019) in 2015 and direct observations from acoustic Doppler current profilers in 2016 confirmed the presence of weak (~1–7 mm s^{-1}) vertical currents, which decreased at night as expected and predicted through scaling analysis in a radiatively driven convective layer (Ulloa et al. 2018).

Here we show the relation between the convective velocity and solar radiation above the ice (Fig. 2a) as well as with solar radiation directly below the ice (Fig. 2b). Note that velocity calculations take into account light attenuation within the water column and are not based solely on the light directly under the ice. Considering the radiation above the ice, the velocities obtained for the same incoming light intensity above ice were much lower in 2016 than 2015, and the relation had a large spread. When the convective velocity was scaled with incoming light below the ice, the data from both years collapsed to the same relation (Fig. 2b). Yet, a correct parameterization of the convective velocity should also take into account the light absorption in the upper water layer (Bouffard et al. 2019). The limited intensity of solar radiation in 2016 resulted in a restricted convective layer (Fig. 2b). These relations show that measuring light under the ice is essential to successful parametrization of under-ice convective mixing. As an example, from an incoming solar radiation above ice of 250 W m^{-2}, and

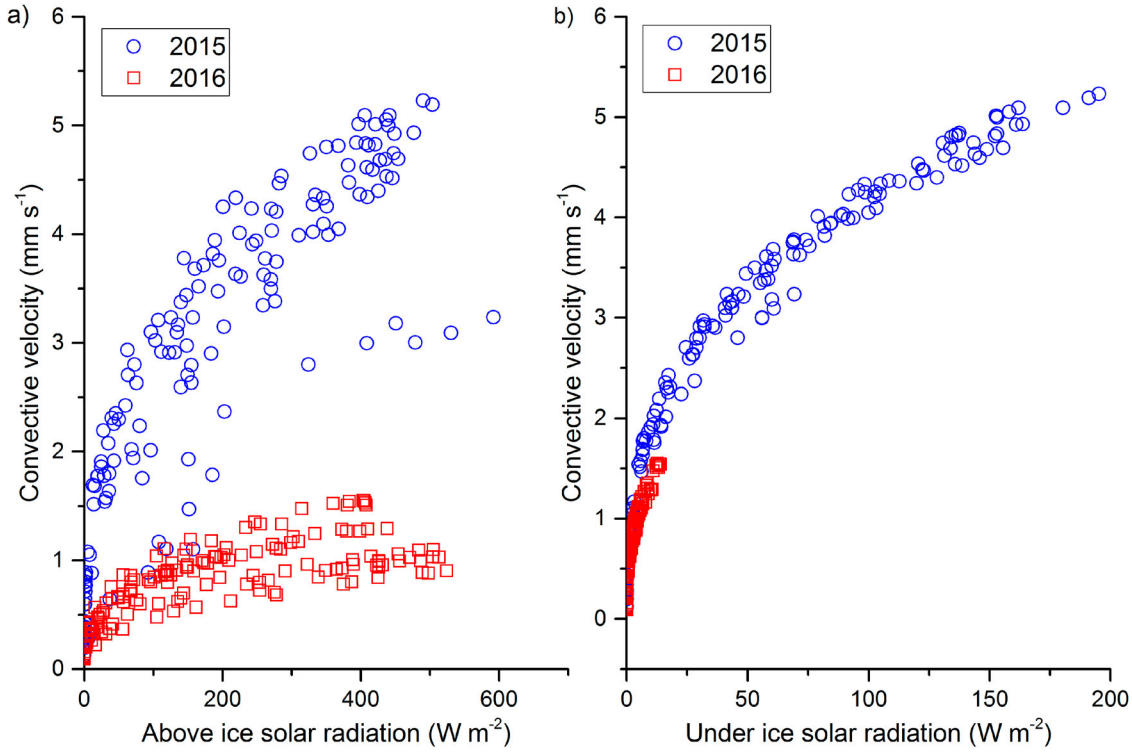

Figure 2. Relations between convective velocity and solar radiation (a) above ice and (b) below ice in March 2015 (blue circles) and in March 2016 (red squares).

assuming a mixed layer thickness of 10 m, the convective velocity can be estimated as $w^* = \sim 4.6$ mm s^{-1} for ice transmittance = 0.4 (in 2015), and PAR attenuation coefficient $k_{PAR} = 1.2$ m^{-1} (in 2015). The convective velocity would only slightly change (to 4.4 mm s^{-1}) using the same 2015 ice transmittance (0.4) but a water attenuation from 2016 ($k_{PAR} = 3.2$ m^{-1}). By contrast, the convective velocity drops to 2.6 mm s^{-1} using the 2016 ice transmittance = 0.07 but the 2015 $k_{PAR} = 1.2$ m^{-1}. In conclusion, the strong attenuation within the snow/ice layer was found to dominate the dynamics of the convective layer (e.g., leading to weaker convective velocity and smaller thickness of convective layer). Yet, the darker water in 2016 also played a minor role in the heat distribution, convective velocity, and ultimately in the convective layer thickness. Thus, under-ice convection is important to consider in our study because vertical mixing patterns may affect the vertical distribution of CO_2 in the water column.

Vertical structure of the water column

In both years, the water column was inversely stratified. In 2015, the convective mixing down to ~24 m had a temperature of 0.95 °C while the bottom water layer had a temperature of 1.5 °C. In 2016, the temperature was 0.10 °C in the convective layer down to ~10 m and reached a maximum temperature of 2.1 °C in the bottom waters (Fig. 3a).

Oxygen profiles (Fig. 3b) had saturation close to 100% over most of the water column in 2016 but at 75–50% near the bottom layer at stations IC and PB3. In 2015, oxygen displayed a similar vertical structure with a depletion in the bottom boundary layer (Fig. 3b).

DOC was homogeneous throughout the water column in 2015, averaging 0.67 mmol L^{-1} (Fig. 4). In 2016, a strong vertical gradient was observed in the bay from ~15 m water depth to the bottom: at station IC, DOC ranged from 1.28 mmol L^{-1} above 15 m but only 0.81 mmol L^{-1} below 15 m. On average, DOC concentrations were higher in 2016 than in 2015.

CO_2 concentrations patterns differed between the 2 years in the vertical distribution in PB (Fig. 5a). In 2016, a distinct vertical structure was observed with 4 different layers: (1) elevated, homogeneous concentrations in the convective layer down to 10 m, averaging 89 (SD 23) µmol L^{-1}; (2) slightly more elevated concentrations between 10 and 15 m, averaging 101 (SD 22) µmol L^{-1}; (3) lower concentrations between 15 and 24 m water depth with an average of 61 (SD 14) µmol L^{-1}; and (4) again higher concentrations near the lake bottom, averaging 86 (SD 34) µmol L^{-1}. In 2015, only 2 layers were observed: layer 1, with homogeneous

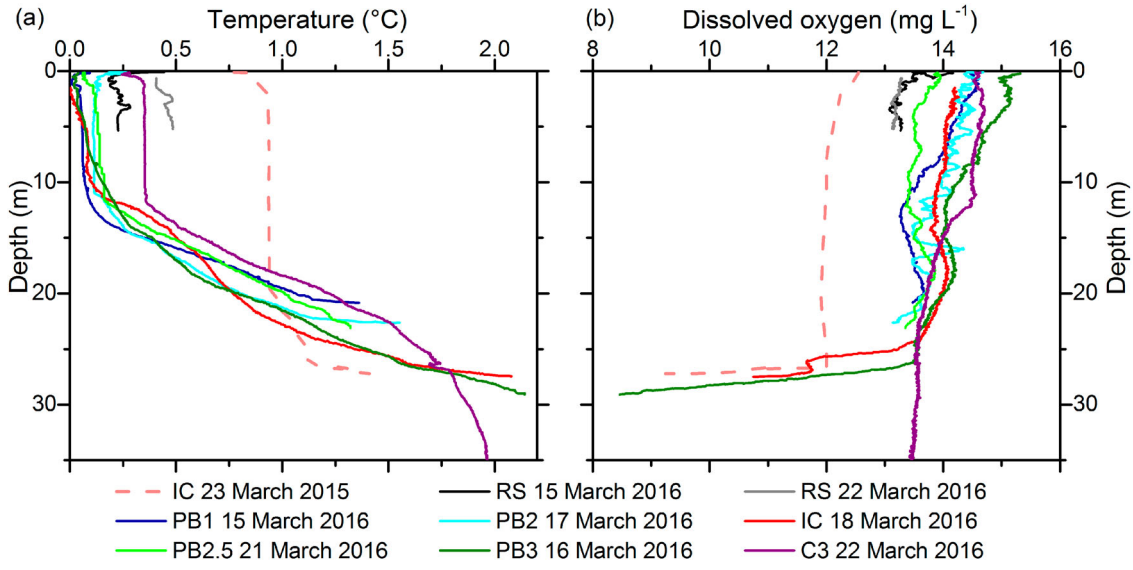

Figure 3. Vertical profiles of (a) temperature and (b) dissolved oxygen in March 2015 (dash line) and in March 2016 (solid lines).

concentrations (49 [SD 5] µmol L^{-1}) in the convective layer between the ice and 24 m water depth and layer 4, with higher concentrations (99 [SD 66] µmol L^{-1}) near the lake bottom.

For both years, DIC concentrations (Fig. 5b) were mostly homogeneous throughout the water column, except for higher values near the lake bottom (>400 µmol L^{-1}).

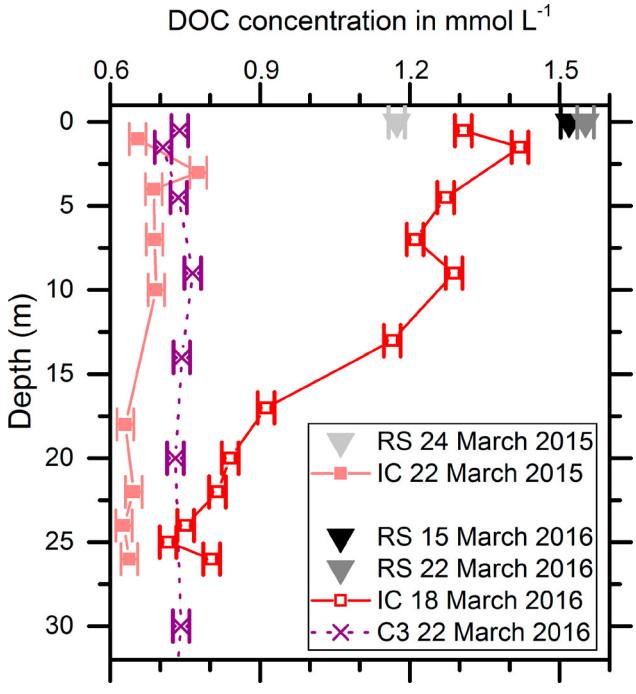

Figure 4. DOC concentration along the river to open-lake transect in March 2015 and 2016. The error bars represent standard deviation.

Spatial distribution along the river to open-lake transect

In 2016, the temperature had a similar horizontal structure at all stations (Fig. 6a), but RS and the top 12 m at C3 were slightly warmer (i.e., denser) than the top 10 m in the bay. Oxygen (Fig. 6b) had a horizontal gradient with lower concentrations between 10 and 15 m depth in PB. Conductivity (Fig. 6c) had a clear horizontal gradient with the lowest value in RS and increasing values in the top 15 m throughout PB. Turbidity also had a distinct gradient along the river to the open-lake transect (Fig. 7a). Turbidity was highest in the river, decreased in the top 15 m throughout PB, and was lowest in the open lake.

In both years, DOC concentrations decreased with increasing distance from RS. In 2015, DOC decreased from 1.18 mmol L^{-1} in the river to 0.67 (SD 0.05) mmol L^{-1} at IC in the bay (Fig 4). In 2016, DOC decreased from 1.55 mmol L^{-1} in the river to 1.04 (SD 0.26) mmol L^{-1} at IC in the bay and 0.73 (SD 0.02) mmol L^{-1} in the open lake (Fig. 4 and 7b). Within PB, the top 15 m had a distinct horizontal gradient. A clear decrease in surface water CO_2 occurred with increasing distance from the river mouth. In 2015, CO_2 decreased from 120 µmol L^{-1} in the river to 51 µmol L^{-1} in PB and 34 µmol L^{-1} in the open lake (Fig. 5a). Similarly, in 2016 CO_2 decreased from 129 µmol L^{-1} in the river to 98 µmol L^{-1} in PB and 36 µmol L^{-1} in the open lake (Fig. 5a and 7c). By contrast, the river had slightly lower DIC concentrations (328 µmol L^{-1}) than the water in the bay and open lake, which had similar concentrations (354 µmol L^{-1}; Fig. 5b) in both years.

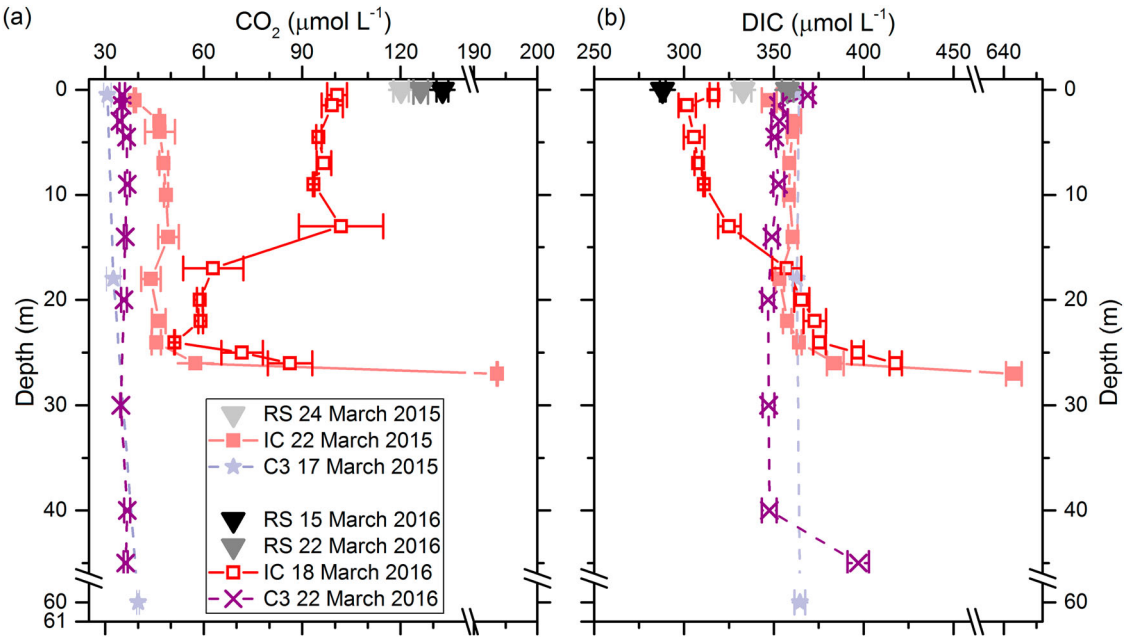

Figure 5. (a) CO_2 and (b) DIC concentrations along a river to open-lake transect in March 2015 and 2016. Error bars represent standard deviation.

Temporal variations in CO_2 concentrations

The high-frequency CO_2 data at 4.5 and 11 m water depth was highly variable. CO_2 concentrations averaged 94.0 (SD 0.9) µmol L^{-1} during the first measurement occasion at 4.5 m depth (Fig. 8a) and 103.8 (SD 14.3) µmol L^{-1} during the second measurement occasion at 11 m depth (Fig. 8b). The variations in temperature (0.22 [SD 0.05] °C) measured at 11 m were used as a proxy for the convective mixing (Fig. 8c). CO_2 concentrations were almost constant (range 4 µmol L^{-1}) at 4.5 m but highly variable, from 79 to 133 (range 54) µmol L^{-1}, at 11 m. The maximum measured concentrations at 11 m were close to the concentration observed in RS. By comparison, the pattern of O_2 concentrations at 11 m were opposite to the pattern of CO_2, with a decrease of O_2 when CO_2 increased and vice versa. At 4.5 m no similar opposing pattern was observed.

The comparison between the 2 years showed contrasting CO_2 distribution, both spatially and vertically. On average, CO_2 concentrations in PB were higher in 2016 than in 2015 while the concentrations in the open lake and the river were similar. The vertical distribution was more homogeneous in 2015 than in 2016.

Discussion

Key processes generating the vertical layering in Petrozavodsk Bay

In PB, vertical profiles of under-ice CO_2 had 4 different layers in 2016 and only 2 in 2015 (Fig. 9). The 4 observed layers can be described as (1) convectively mixed layer down to ~10 m, (2) a layer with higher CO_2 from ~10 to 15 m, (3) an intermediate layer low in CO_2 from ~15 to 2 m above the sediment, and (4) the benthic boundary layer for the lowermost 2 m. The main difference in 2015 was the absence of layers 2 and 3 because the intense convective mixing homogenized concentrations over the entire convective layer down to ~24 m. Bouffard et al. (2019) showed that the extent of under-ice convection varied between winters because of the penetrating solar radiation driven by ice conditions, and because the increase in DOC only marginally affected the dynamic of the convective layer. Convective mixing is therefore a key process affecting the concentration and vertical distribution of CO_2 below the ice.

In 2016, slightly higher concentrations of CO_2 were observed in layer 2, which we interpreted as an intrusion of riverine water. This CO_2-rich layer (2) is located between the convective layer (1) and the CO_2-poor layer (3), and thus must be maintained by an active process such as horizontal advection. This horizontal transport from the river is further supported by spatial distributions of turbidity, oxygen, conductivity, DOC, and CO_2 (Fig. 6b–c and 7). Hence, the river intrusion seems to constitute an important input of CO_2 and DOC into the bay. This layer was probably already partially mixed by the convective mixing during the sampling campaign in 2016, which makes it more difficult to differentiate. We expect that in early spring, the convective mixing

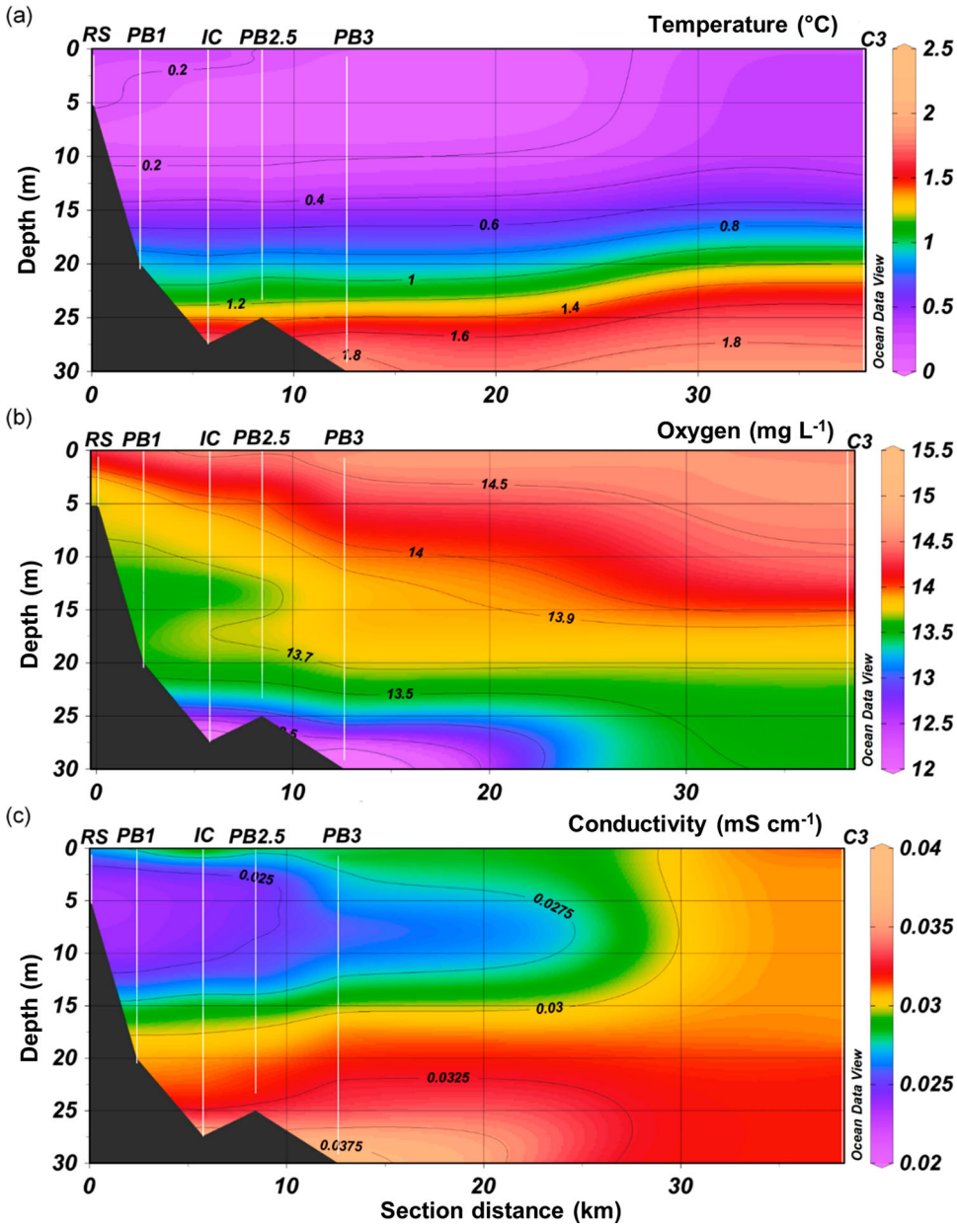

Figure 6. Vertical distribution interpolated along the river to open-lake transect on 20, 22, and 23 March 2016 of (a) temperature, (b) oxygen, and (c) conductivity. White vertical lines show the measured profiles.

would generally be shallow because of low solar insolation and because a river plume, being colder thus denser, would be more likely to intrude below the convective mixed layer. In late spring, as the convective cells reach greater depths, the river intrusion would probably be homogenized throughout most of the water column, similar to 2015.

Layer 3 was characterized by low DOC and CO_2 concentrations, similar to values measured in the pelagic waters. Sabylina et al. (2010) also described a distinct water layer in the bay similar to the open lake and frequently observed under the ice between 15 and 20 m. This water layer is probably remnant water from past autumn turnover, which homogenized the entire water column at lower CO_2 concentrations (Bellido et al. 2009, Ducharme-Riel et al. 2015). At these depths, water is isolated from any CO_2 inputs from the sediment and the river and is therefore likely to reflect CO_2 concentrations close to the last mixing event.

Below layer 3, the benthic boundary layer (4) was similar in extent in 2015 and 2016 and characterized by high concentrations of CO_2 (Fig. 5a and 7c) and of DIC (Fig. 5b). The high CO_2 in this layer results from mineralization of organic matter in the sediment, which releases DIC and consumes O_2 (Fig. 3b

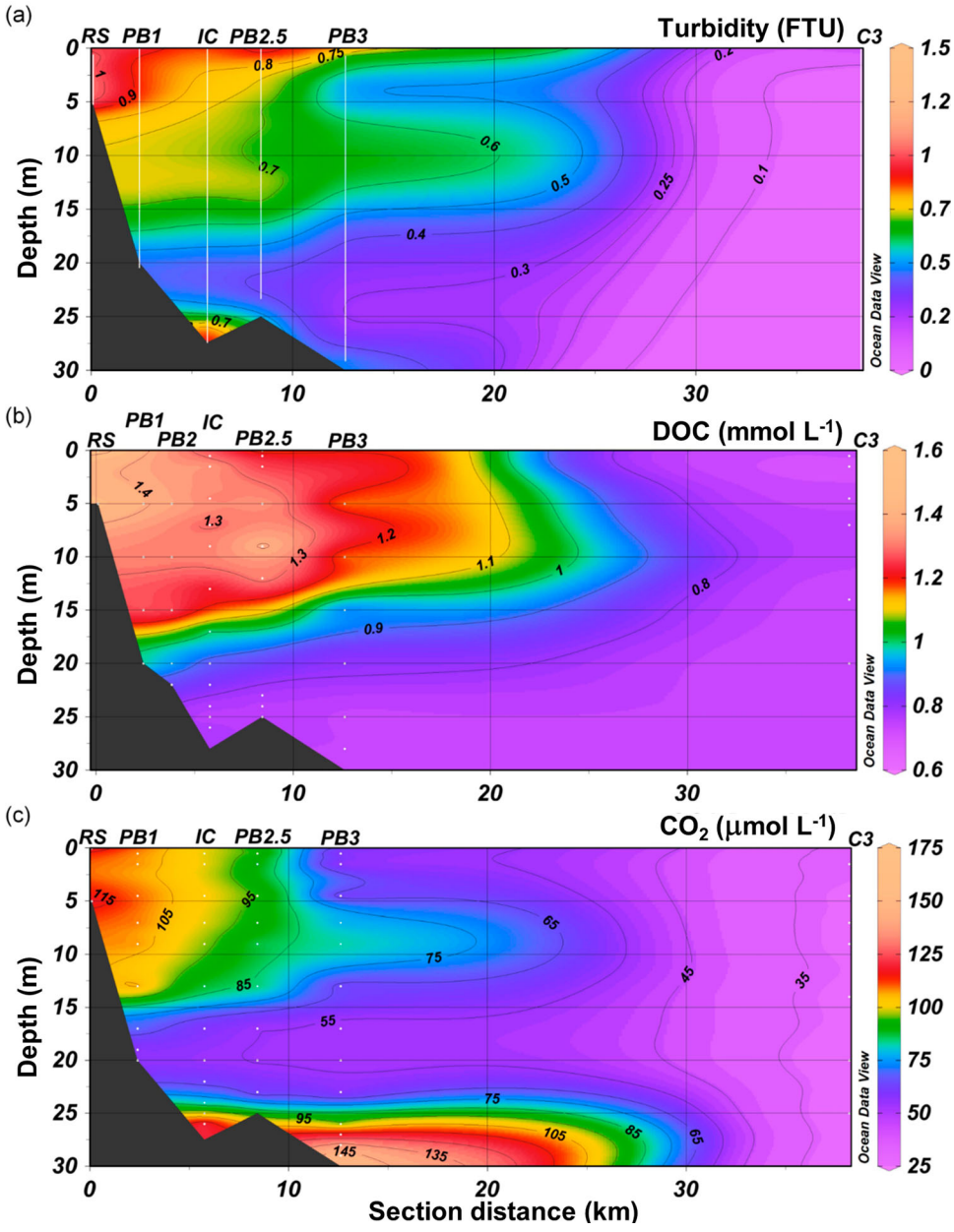

Figure 7. Vertical distribution interpolated along the river to open-lake transect (a) of turbidity on 20, 22, and 23 March 2016. (b) DOC concentrations on 21 and 22 March, except IC on 18 March 2016. (c) CO_2 concentrations measured using Contros CO_2 sensor on 20, 22, and 23 March. White points show the depth and location of measurements.

and 5). Sediment respiration is an important input of DIC to the water column, and CO_2 accumulation in deep water during winter has often been recorded for boreal lakes (Jonsson et al. 2001, Denfeld et al. 2015).

In conclusion, a shallow convective mixing reaching the suggested signal from RS explains the higher heterogeneity within the water column in 2016. In 2015, the intense convective mixing homogenized most of the water column, leaving only the deepest layer to accumulate CO_2 diffused from the sediment. The key processes explaining these structures are therefore under-ice convective mixing, horizontal transport assimilated to the river intrusion, and sediment respiration.

Spatial gradient in CO_2 concentrations

CO_2 and DOC concentrations decreased with increasing distance from the river mouth in both years (Fig. 4, 5a, and 7b–c). RS had higher CO_2 concentrations than PB by a factor 2.5 in 2015 and 1.5 in 2016, representing 95% of the bay water inputs. Hence, RS seems to discharge important loads of CO_2 and DOC to PB, which are progressively diluted in the bay with increasing distance from the river mouth.

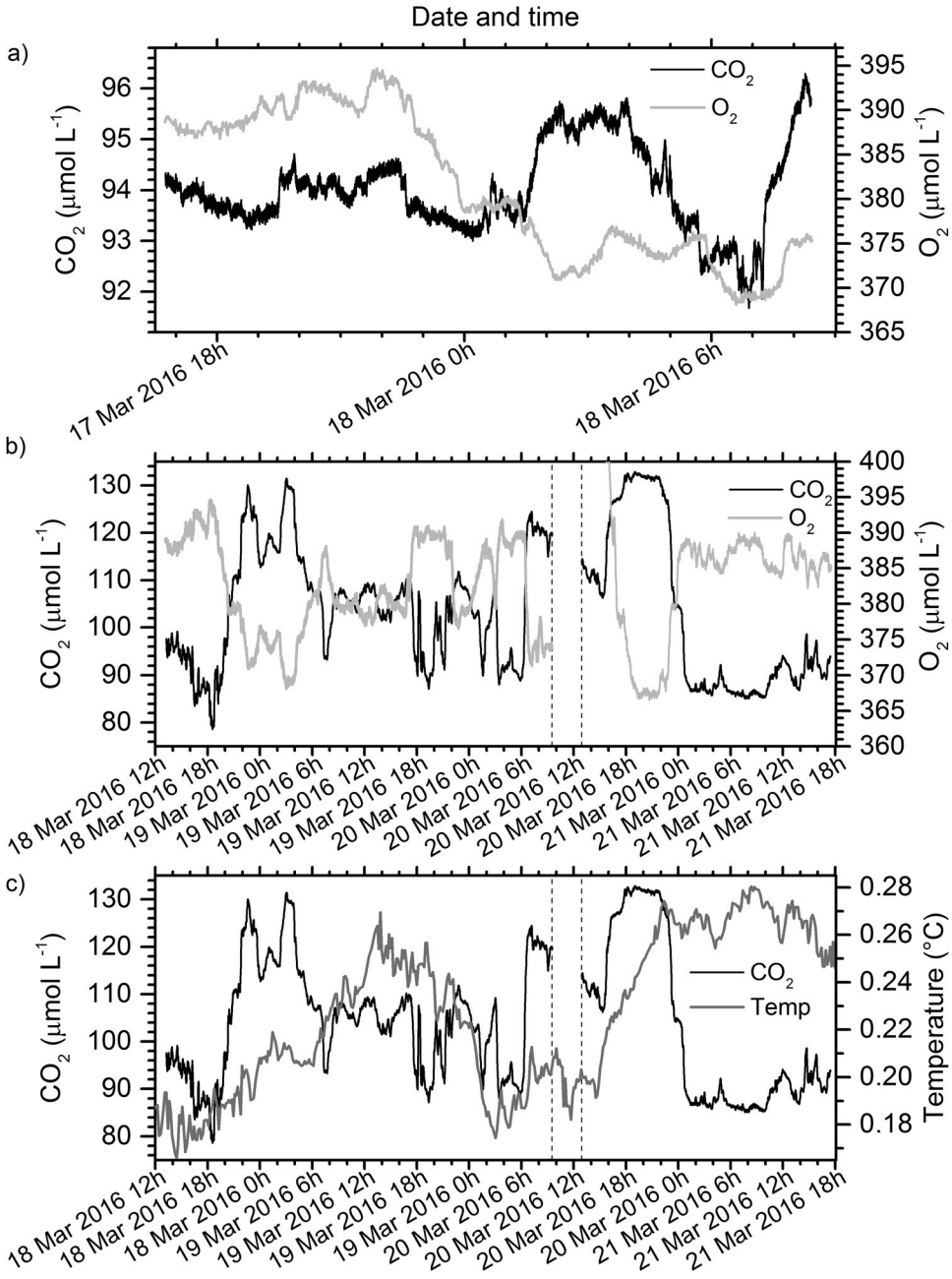

Figure 8. Concentrations of CO_2 and O_2 at (a) 4.5 m overnight from 17 to 18 March, and (b) 11 m depth during 18 and 21 March 2016. (c) Concentrations of CO_2 and temperature (°C) at 11 m depth during 18 and 21 March 2016.

This study supports previous evidence that rivers have higher DOC (Cortés et al. 2017) and CO_2 concentrations than lakes (Crawford et al. 2014, Kokic et al. 2015). The high DOC concentrations in RS provide substrate for microbial degradation of terrestrial DOC and thereby stimulate in situ CO_2 production. In addition, rivers typically receive a large contribution of water from groundwater and therefore high CO_2 inputs from terrestrial soil respiration (Maberly et al. 2012). By contrast, large lakes typically receive a smaller share of groundwater-derived CO_2 because of the small contribution from the catchment compared to the large volume of the lake. In our study, it seems plausible that respiration contributes to the higher CO_2 concentrations in RS, which is an important direct source of CO_2 to Lake Onego.

While most studies have compared CO_2 in rivers and lakes, we identified the river signal throughout the river inflow area of a large bay of Lake Onego. This transition zone between the river and the lake is characterized by high spatial variability in CO_2 (Fig. 7c) compared to the more stable conditions in the open lake (Fig. 5a). Because Lake Onego has >1000 tributaries, we expect that the near-shore areas of this large lake are generally characterized by high dynamics. These dynamics might

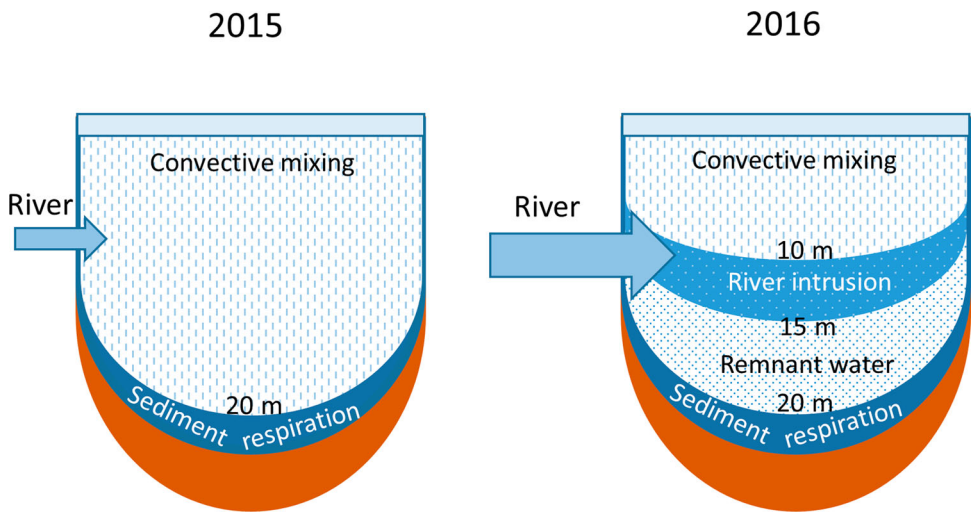

Figure 9. Conceptual scheme of the changes in vertical layering and processes in Petrozavodsk Bay between years (a) 2015 and (b) 2016.

be similar to PB, especially for the 2 other largest rivers, Vodla and Suna. For the other 52 rivers longer than 10 km, these effects might extend closer to the shoreline, whereas the other smaller tributaries might only have local effects. This finding of high spatial heterogeneity of CO_2 shows that the usual one point-in-time measurement in the deepest part of a lake would clearly underestimate the lake CO_2 budget, calling for more spatially resolved samplings.

Processes explaining the temporal variations

Pronounced short-term variations

Our high-frequency CO_2 measurements revealed pronounced dynamics at short time scales (±50 µmol L^{-1} within 4 h) especially at 11 m (Fig. 8). Other under-ice studies with similar sensors also indicated that high temporal variability of under-ice CO_2 and O_2 concentrations can occur and were mostly explained by a combination of biological and physical processes (Baehr and DeGrandpre 2002, 2004, Denfeld et al. 2015, Obertegger et al. 2017). In our study, the large variations might instead be driven by mixing of different water masses rather than by biological processes. First, CO_2 and O_2 signals at 11 m had opposing temporal patterns with irregular occurrences, incongruent with diurnal patterns driven by photosynthesis and respiration. Photosynthesis can be excluded because light is absent at this depth, and respiration is probably not highly variable because substrate supply from primary production is absent and temperature is low and stable (0.22 [SD 0.05] °C; Fig. 8c). Second, the observed oscillations are probably not linked to convective mixing because they are not correlated with temperature (Fig. 8c). Rather than vertical mixing, this temporal pattern is probably induced by horizontal transport. We suggest that these short-term variations are related to the signal from the river measured by the sensor intermittently within the bay water. RS was ~25 µmol L^{-1} more depleted in O_2 and ~45 µmol L^{-1} more enriched in CO_2 compared to the bay water (Fig. 3b and 5a), corresponding to the observed difference between extreme values. As such, RS may possibly intrude within the bay along different trajectories, such that the CO_2 sensor caught the river signal only when it was in the direct trajectory of the river plume. While the river inflow is clearly discharging in the bay, the exact trajectory of the river intrusion cannot be assessed with current data. In conclusion, RS not only affects the vertical structure of the water column (compared with layer 2), but might also create additional heterogeneity in the horizontal plane.

Comparison between years

Our study revealed a marked variability between winters, with higher DOC and CO_2 concentrations in PB in 2016 than in 2015. This variability in CO_2 is probably explained by the river load, which was 2 times higher in 2016 (129 µmol L^{-1}, 47.7 m^3 s^{-1}) than in 2015 (120 µmol L^{-1}, 25.2 m^3 s^{-1}; Table 1). In a catchment dominated by forest, such as RS, DOC inputs usually rise when the river discharge increases (Laudon et al. 2011). Larger discharge enhances groundwater mobilization, and thus more groundwater reaches the river, increasing the export of DOC and CO_2 from the catchment. The hydrology, and thus the discharge from RS, are important for the CO_2 distribution within the bay and the amount of CO_2 below the ice.

However, the ice quality (clear or covered with snow) determines the amount of solar radiation penetrating the water column, which in turn regulates the strength, magnitude, and temporal course of convective mixing (Bouffard et al. 2019). The homogeneity within the water column driven by convective mixing might strongly reduce surface CO_2 and thus the potential emissions at ice-melt. This scenario is especially true if the water column is entirely mixed below the ice as opposed to during the ice break-up. Indeed, water column mixing upon ice-melt tends to release CO_2 that accumulated in bottom waters directly into the atmosphere (Denfeld et al. 2018).

In summary, the observed changes in discharge and convective mixing between winters led to different spatiotemporal pattern within the bay area, which may have a strong effect on the CO_2 emission at ice break-up.

Comparison with other ice-covered lakes

Under-ice CO_2 concentrations in Lake Onego are at the lower range of CO_2 reported in previous studies. Surface CO_2 ranged from 51 to 98 µmol L^{-1} in PB while small boreal lakes had concentrations of 100 µmol L^{-1} (Ducharme-Riel et al. 2015), 92 to 213 µmol L^{-1} (Denfeld et al. 2015), 60 to 180 µmol L^{-1} (Miettinen et al. 2015), and even 300 µmol L^{-1} (Demarty et al. 2001). By comparison, CO_2 in the open lake was significantly lower at only 35 µmol L^{-1}. However, these studies investigated small lakes with much smaller volumes than Lake Onego, or even PB. In large lakes, lateral CO_2 inputs are generally less important than in small lakes, as we also noted between PB and the open lake.

In PB bottom waters, CO_2 reached a maximum of 120 µmol L^{-1} in 2016 and 194 µmol L^{-1} in 2015. Other reported values reached 310 µmol L^{-1} (Miettinen et al. 2015), 120 to 300 µmol L^{-1} (Denfeld et al. 2015), and even 450 µmol L^{-1} (Ducharme-Riel et al. 2015). Thus, Lake Onego had lower bottom CO_2 concentrations than previous studies in smaller lakes. Bottom CO_2 accumulation is mostly caused by mineralization of organic matter in the sediment. The importance of this mineralization is higher in small lakes, given their larger proportion of sediment area compared to the lake volume.

As in other lakes, CO_2 concentrations in Lake Onego were significantly higher under-ice than in early spring. A forthcoming study (H.E. Chmiel, unpubl.) will further investigate how the observed under-ice spatiotemporal distribution in winter affects CO_2 emission at ice break-up. A limitation of our study is that the single campaign at the end of winter provides only a snapshot of under-ice conditions, preventing evaluation of CO_2 evolution throughout winter and during ice-melt. However, our study is innovative because it simultaneously measures physical processes and biogeochemistry for the first time in a large frozen lake. In future studies, physical and biochemical models (Baehr and DeGrandpre 2004) could be used to quantify the contribution of different processes to the observed CO_2. In addition, the interannual variability should be assessed throughout the entire ice-covered period.

Conclusions

Our study shows that river inflow, under-ice convective mixing, and sediment respiration are the key drivers of under-ice CO_2 concentration patterns. Measuring under-ice convection simultaneously with CO_2 seems to be essential to explain the spatiotemporal variations in under-ice CO_2 because under-ice convection is probably a widespread process in lakes covered by ice with limited snow. Depending on the intensity of penetrating solar radiation, this efficient vertical mixing could homogenize the water column as deep as 25 m, corresponding to a complete overturn in most shallow lakes. Such overturn already below the ice might reduce emissions at ice-melt.

This study also indicates that the inflowing river is an important source of CO_2 to the bay and causes marked CO_2 dynamics in space and time. This transition zone between the river and the lake is therefore characterized by strong CO_2 variability. In large lakes, it is therefore essential to consider river inflow areas. Measuring only in the pelagic waters might underestimate the lake CO_2 budget as well as the lake potential emissions at ice break-up.

Disclosure statement

No potential conflict of interest was reported by the author(s).

Acknowledgements

The authors thank the "Fondation pour l'Etude des Eaux du Léman" for funding the project "Life under ice" that took place in Lake Onego from 2015 to 2017. SS acknowledges funding from the European Research Council under the European Union's Seventh Framework Programme (FP7/2007-2013)/ERC grant agreement n° 336642. We express special thanks to the Limnology Center from EPFL and the Northern Water Problems Institute (NWPI) from the Russian Academy of Sciences in Karelia for providing technical and logistical support during field expeditions. We especially thank Nikolay Filatov, Roman Zdorovennov, and Vasily Kovalenko for the excellent coordination of the field expeditions. We thank the hydrochemical team from NWPI, especially Michael V. Kalmykov, Olga I. Ikko, and Tatyana A. Efremova for

their help during sampling and their local knowledge of Lake Onego. The authors also thank AuA laboratory at Eawag for DOC measurements. We are also grateful to Blaize Denfeld for her advice on the methodology and study design. Finally, we thank the whole team of "Life Under Ice" project for their commitment and interdisciplinary inputs.

ORCID

Natacha Pasche http://orcid.org/0000-0002-9578-9301
Hilmar Hofmann http://orcid.org/0000-0001-6140-5886
Damien Bouffard http://orcid.org/0000-0002-2005-9718
Carsten J. Schubert http://orcid.org/0000-0003-1668-5967
Petr A. Lozovik http://orcid.org/0000-0002-0062-2235
Sebastian Sobek http://orcid.org/0000-0003-1351-9277

References

Baehr MM, DeGrandpre MD. 2002. Under-ice CO_2 and O_2 variability in a freshwater lake. Biogeochemistry. 61:95–11.

Baehr MM, DeGrandpre MD. 2004. In situ pCO_2 and O_2 measurements in a lake during turnover and stratification: observations and modelling. Limnol Oceanogr. 49:330–340.

Bellido L, Tulonen JT, Kankaala P, Ojala A. 2009. CO_2 and CH_4 fluxes during spring and autumn mixing periods in a boreal lake (Pääjärvi, southern Finland). J Geophys Res. 114:G04007.

Bizic'-Ionescu M, Amann R, Grossart HP. 2014. Massive regime shifts and high activity of heterotrophic bacteria in an ice-covered lake. PLOS ONE. 9:1–17.

Bouffard D, Zdorovennov RE, Zdorovennova GE, Pasche N, Wüest A, Terzhevik AY. 2016. Ice covered Lake Onega: effects of radiation on convection and internal waves. Hydrobiologia. 780:21–36.

Bouffard D, Zdorovennova GE, Bogdanov S, Efremova T, Lavanchy S, Palshin N, Terzhevik AY, Råman Vinnå L, Volkov S, Wüest A. et al. 2019. Under-ice convection dynamics in a boreal lake. Inland Waters. 9(2):142–161. doi:10.1080/20442041.2018.1533356.

Bouffard D, Wüest A. 2019. Convection in Lakes. Annu Rev Fluid Mech. 51:189–215.

Chmiel HE, Kokic J, Denfeld BA, Einarsdóttir K, Wallin MB, Koehler B, Isidorova A, Bastviken D, Ferland M-È, Sobek S. 2016. The role of sediments in the carbon budget of a small boreal lake. Limnol Oceanogr. 61:1814–1825.

Cortés A, MacIntyre S, Sadro S. 2017. Flowpath and retention of snowmelt in an ice-covered arctic lake. Limnol Oceanogr. 62:2023–2044.

Crawford JT, Lottig NR, Stanley EH, Walker JF, Hanson PC, Finlay JC, Striegl RG. 2014. CO_2 and CH_4 emissions from streams in a lake-rich landscape: patterns, control, and regional significance. Global Biogeochem Cy. 28:1–14.

Denfeld BA, Baulch HM, Del Giorgio PA, Hampton SE, Karlsson J. 2018. A synthesis of carbon dioxide and methane dynamics during the ice-covered period of northern lakes. Limnol Oceanogr Lett. 3:117–131.

Denfeld BA, Kortelainen P, Rantakari M, Sobek S, Weyhenmeyer GA. 2015. Regional variability and drivers of below ice CO_2 in boreal and subarctic lakes. Ecosystems. 19:461–676.

Demarty M, Bastien J, Tremblay A. 2001. Annual follow-up of gross diffusive carbon dioxide and methane emissions from a boreal reservoir and two nearby lakes in Québec, Canada. Biogeosciences. 8:41–53.

Duarte CM, Prairie YT. 2005. Prevalence of heterotrophy and atmospheric CO_2 emissions from aquatic ecosystems. Ecosystems. 8:862–870.

Ducharme-Riel V, Vachon D, Del Giorgio PA, Prairie YT. 2015. The relative contribution of winter under-ice and summer hypolimnetic CO_2 accumulation to the annual CO_2 emissions from northern lakes. Ecosystems. 18:547–559.

Filatov N, Baklagin V, Balagansky A, Efremova T, Nazarova L, Palshin N. 2019. Climate change impacts on the watersheds of Lakes Onego and Ladoga from remote sensing and in situ data. Inland Waters. 9(2):130–141. doi:10.1080/20442041.2018.1533355.

Golub M, Desai AR, McKinley GA, Remucal CK, Stanley EH. 2017. Large uncertainty in estimating pCO_2 from carbonate equilibria in lakes. J Geophys Res-Biogeosci. 122:2909–2924.

Hampton SE, Moore MV, Ozersky T, Stanley E H, Polashenski CM, Galloway AWE. 2015. Heating up a cold subject: prospects for under-ice plankton research in lakes. J Plankton Res. 37:277–284.

Jonsson A, Meili M, Bergström A-K, Jansson M. 2001. Whole-lake mineralization of allochthonous and autochthonous organic carbon in a large humic lake (Örträsket, N. Sweden). Limnol Oceanogr. 46:1691–1700.

Karlsson J, Giesler R, Persson J, Lundin E. 2013. High emission of carbon dioxide and methane during ice thaw in high latitude lakes. Geophys Res Lett. 40:1123–1127.

Kokic J, Wallin MB, Chmiel HE, Denfeld BA, Sobek S. 2015. Carbon dioxide evasion from headwater systems strongly contributes to the total export of carbon from a small boreal lake catchment. J Geophys Res Biogeosci. 120:13–28.

Laudon H, Berggren M, Ågren A, Buffam I, Bishop K, Grabs T, Jansson M, Köhler S. 2011. Patterns and dynamics of dissolved organic carbon (DOC) in boreal streams: the role of processes, connectivity, and scaling. Ecosystems. 14:880–893.

Leppäranta M. 2015. Freezing of lakes. Freezing of lakes and the evolution of their ice cover. Berlin Heidelberg (Germany): Springer; p. 11–50.

Lozovik PA, Morozov AK, Zobkov MB, Dukhovicheva TA, Osipova LA. 2007. Allochthonous and autochthonous organic matter in surface waters in Karelia. Water Resour. 34:204–216.

Maberly SC, Barker PA, Stott AW, De Ville MM. 2012. Catchment productivity controls CO_2 emissions from lakes. Nat Clim Change. 3:391–394.

Miettinen H, Pumpanen J, Heiskanen JJ, Aaltonen H, Mammarella I, Ojala A, Levula J, Rantakari M. 2015. Towards a more comprehensive understanding of lacustrine greenhouse gas dynamics – two-year measurements of concentrations and fluxes of CO_2, CH_4 and N_2O in a typical boreal lake surrounded by managed forests. Boreal Env Res. 20:75–89.

Natchimuthu S, Sundgren I, Gålfalk M, Klemedtsson L, Bastviken D. 2017. Spatiotemporal variability of lake pCO_2 and CO_2 fluxes in a hemiboreal catchment Sivakiruthika. J Geophys Res-Biogeosci. 122:30–49.

Obertegger U, Obrador B, Flaim G. 2017. Dissolved oxygen dynamics under ice: three winters of high-frequency data from Lake Tovel, Italy. Water Resour Res. 53:7234–7246.

Podsechin V, Kaipainen H, Filatov N, Bilaletdin Ä, Frisk T, Paananen A, Terzhevik A, Vuoristo H. 2009. Development of water protection of Lake Onega. Suomen Ympäristö 36. https://helda.helsinki.fi/handle/10138/38020

Powers SM, Hampton SE. 2016. Winter limnology as a new frontier. Limnol Oceanogr Bull. 25:103–108.

Sabylina AV, Lozovik PA, Zobkov MB. 2010. Water chemistry in Onega lake and its tributaries. Water Resour. 37:842–853.

Sobek S, Algesten G, Bergström A-K, Jansson M, Tranvik LJ. 2003. The catchment and climate regulation of pCO_2 in boreal lakes. Global Change Biol. 9:630–641.

Stets EG, Striegl RG, Aiken GR, Rosenberry DO, Winter TC. 2009. Hydrologic support of carbon dioxide flux revealed by whole-lake carbon budgets. J Geophys Res-Biogeosci. 114:G01008.

Tranvik LJ, Downing JA, Cotner JB, Loiselle SA, Striegl RG, Ballatore TJ, Dillon P, Finlay K, Fortino K, Knoll LB, et al. 2009. Lakes and reservoirs as regulators of carbon cycling and climate. Limnol Oceanogr. 54:2298–2314.

Ulloa HN, Wüest A, Bouffard D. 2018. Mechanical energy budget and mixing efficiency for a radiatively heated ice-covered waterbody. J Fluid Mech. 852:R1.

Weiss RF. 1974. Carbon dioxide in water and seawater: the solubility of a non-ideal gas. Mar Chem. 2:203–215.